- 1 Quantifying the Role of the Relative-Humidity Dependent Physical State of Organic
- 2 Particulate Matter on the Uptake of Semivolatile Organic Molecules

3

- 4 Yuemei Han,\*,†,‡ Zhaoheng Gong,† Jianhuai Ye,† Pengfei Liu,† Karena A. McKinney,†,§ and Scot
- 5 T. Martin\*,†,||

6

- 7 †School of Engineering and Applied Sciences, Harvard University, Cambridge, Massachusetts
- 8 02138, United States
- 9 <sup>‡</sup>Key Laboratory of Aerosol Chemistry and Physics, State Key Laboratory of Loess and
- 10 Quaternary Geology, Institute of Earth Environment, Chinese Academy of Sciences, Xi'an,
- 11 Shaanxi 710061, China
- 12 Department of Earth and Planetary Sciences, Harvard University, Cambridge, Massachusetts
- 13 02138, United States
- 14 §Present Address: Department of Chemistry, Colby College, Waterville, Maine 04901, United
- 15 States

16

- 17 \*Corresponding Authors: Scot T. Martin (scot martin@harvard.edu) and Yuemei Han
- 18 (yuemei.han@ieecas.cn).

19

- 20 Environmental Science & Technology
- 21 Submitted: September 2019
- The authors declare no competing financial interest.

#### **ABSTRACT**

24

25

26

27

28

29

30

31

32

33

34

35

36

37

38

39

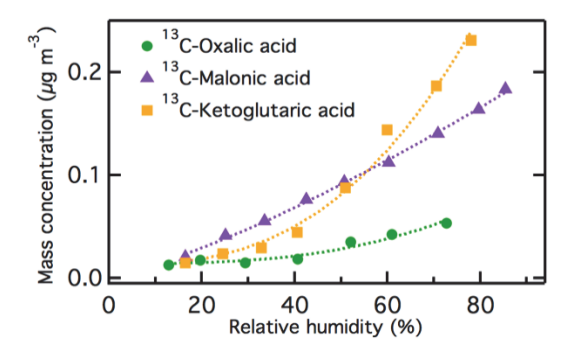
40

The uptake of gas-phase dicarboxylic acids to organic particulate matter (PM) was investigated to probe the role of PM physical state on exchange processes between gas-phase semivolatile organic molecules and organic PM. A homologous series of probe molecules, specifically isotopically labeled <sup>13</sup>C-dicarboxylic acids, was used in conjunction with aerosol mass spectrometry to obtain a quantitative characterization of the uptake to organic PM for different relative humidities (RH). The PM was produced by the dark ozonolysis of unlabeled αpinene. The uptake of  $^{13}$ C-labeled oxalic, malonic, and  $\alpha$ -ketoglutaric acids increased stepwise by 5 to 15 times with increases in RH from 15% to 80%. The enhanced uptake with increasing RH was explained primarily by the higher molecular diffusivity in the particle phase, as associated with changes in the physical state of the organic PM from a non-liquid state to a progressively less-viscous liquid state. At high RH, the partitioning of the probe molecules to the particle phase was more associated with physicochemical interactions with the organic PM than with the co-absorbed liquid water. Uptake of the probe molecules also increased with a decrease in volatility along the homologous series. This study quantitatively shows the key roles of particle physical state in governing the interactions of organic PM with semivolatile organic molecules.

41

42

**Keywords:** Dicarboxylic acids, isotopic labeling,  $\alpha$ -pinene ozonolysis, organic particulate matter, physical state, diffusivity, volatility.



#### 1. INTRODUCTION

47

48

49

50

51

52

53

54

55

56

57

58

59

60

61

62

63

64

65

66

67

68

69

Atmospheric organic particulate matter (PM) consists in substantial part of secondary products from the oxidation of volatile organic compounds. Organic PM is of great importance to the Earth's climate and human health.<sup>2,3</sup> Organic PM can have variable viscosities (i.e., physical state) ranging from solids, to semisolids, to liquids.<sup>4,5</sup> The physical state can vary and change with environmental factors such as relative humidity and temperature as well as chemical factors such as hydrocarbon precursor and the history of reaction chemistry. 6-10 In this context. relative humidity can be regarded as a particularly important variable among the controlling factors. 11,12 The physical state of organic PM has been characterized by multiple techniques via directly and indirectly measuring particle viscosity. <sup>7,10,13–15</sup> The dynamic exchange of gas-phase organic molecules, such as organic nitrates, polycyclic aromatic hydrocarbons, and levoglucosan, has been demonstrated to be kinetically limited for sufficiently low relative humidity by the physical state of organic PM, 16-20 which can also affect the further chemical reactions taken place after uptake. There are many different organic molecules present in the atmosphere, whereas the possible roles of organic PM physical state in the interactions between gas-phase and particle-phase organic molecules remain poorly understood. Ubiquitous semivolatile organic compounds (SVOCs) are an important source of organic PM in the atmosphere. SVOCs have saturation concentrations from  $10^{-1}$  to  $10^3$  µg m<sup>-3</sup>, and they dynamically partition between the gas and particle phases under typical atmospheric conditions.<sup>21</sup> Partitioning of SVOCs between the gas and particle phases is one of the key processes for predicting the mass concentration of ambient organic PM in the submicron particle size range. 22,23 Gas-particle partitioning is traditionally assumed to be an effectively instantaneous process, yet this assumption is challenged by findings regarding the viscosity and

the physical state of organic PM. For instance, the uptake of semivolatile organic nitrates was kinetically limited due to the high viscosity of the organic PM. <sup>16,18,19</sup> SVOCs such as polycyclic aromatic hydrocarbons can be trapped inside highly viscous semisolid organic PM, and further evaporation and oxidation can thus be hindered. <sup>17,24</sup> Moreover, the physical and chemical properties of SVOCs, such as their diffusivity, volatility, and chemical structure, can be important factors controlling the gas-particle interactions. A transition from a kinetically limited to a thermodynamically limited regime can take place, as observed for example in the uptake of levoglucosan by α-pinene-derived organic PM. <sup>20</sup> Overall, the influence of PM physical state and the related dependencies on SVOC molecular diffusivity and SVOC volatility on the dynamic exchange and reactivity between organic PM and gas-phase species has been demonstrated as important, yet these factors and interactions remain to be fully quantitatively understood and characterized.

Dynamic exchange of species between the gas and particle phases is an important process that ultimately affects the transformation, evolution, and environmental fate of atmospheric PM. Heterogeneous interactions of various gas species have been investigated extensively. A major focus has been on the uptake of water vapor, reactive free radicals (e.g., OH, HO<sub>2</sub>, and NO<sub>3</sub>), and trace gases of small molecules (e.g., NH<sub>3</sub> and O<sub>3</sub>).<sup>25</sup> Previous studies have also provided fundamental knowledge on the multiphase chemistry of gas-phase organic species such as glyoxal, methylglyoxal, pinonaldehyde, and isoprene-derived epoxydiols, especially for inorganic particles.<sup>26–30</sup> The uptake of gas-phase semivolatile organic molecules to organic PM can have different governing factors, in particular when taking into account viscosity and particle-phase reactions. One of the major challenges in characterizing this type of uptake is to track and differentiate the probe molecules once they have interacted with the host organic

matrix in the particle phase. Stable isotope labeling of either probe molecules or organic PM, in conjunction with mass spectrometry, provides one strategy to distinguish probe molecules in a mixture of organic materials.<sup>31–34</sup>

The present study investigates the dynamic exchange between gas-phase semivolatile organic molecules and organic PM. Isotopically labeled dicarboxylic acids are used as the gas-phase probe molecules. Dicarboxylic acids are commonly present in the atmosphere at significant concentrations as the result of oxidation processes, and their uptake may lead to substantial changes in PM hygroscopicity and light-absorption. Dicarboxylic acids originate in large part from atmospheric photochemical reactions in aqueous phase and to a lesser extent from biomass burning and fossil fuel combustion. Herein, the diffusive uptake of gas-phase dicarboxylic acid molecules by  $\alpha$ -pinene-derived organic PM was studied across variable relative humidity (RH). Isotopically labeled <sup>13</sup>C-dicarboxylic acids were used for identifying and quantifying the uptake in the particle phase using on-line aerosol mass spectrometry. The roles of RH-dependent organic PM physical state and associated diffusivity of probe molecules on the uptake process were studied.

#### 2. MATERIALS AND METHODS

#### 2.1. Isotopically Labeled Dicarboxylic Acids.

A homologous series of fully isotopically labeled  $^{13}$ C dicarboxylic acids served as the gasphase probe semivolatile organic compounds. The compounds included oxalic, malonic, and adipic acids, which are saturated linear dicarboxylic acids, as well as the functionalized compound of  $\alpha$ -ketoglutaric acid. Table 1 summarizes the physical and chemical properties. The isotopic enrichment was > 99% for all compounds (Cambridge Isotope Laboratories, Inc., Andover, Massachusetts, USA). The isotopically labeled dicarboxylic acids can be expected to

exhibit nearly identical physicochemical properties as those of unlabeled ones because  $^{12}$ C and  $^{13}$ C have the same number of electrons and share a similar electronic structure. The saturation concentrations of these probe compounds ranged from 13 to 1018  $\mu$ g m<sup>-3</sup>,<sup>36</sup> representing the mid- to upper end of the semivolatile range.  $^{21,37}$ 

Prior to the uptake experiments, tracer fragments in the mass spectrum of each probe compound in the particle phase were identified. For this purpose, a polydisperse population of  $^{13}$ C-labeled particles of a single compound was produced by the atomization of an aqueous solution (0.1 g L $^{-1}$ ) using an aerosol generator (model 3076, TSI Inc.) at an air flow of 2.5 L min $^{-1}$ . The resulting flow passed through a silica gel diffusion dryer, and the aerosol particles in the flow were characterized by an on-line high-resolution time-of-flight aerosol mass spectrometer (HR-ToF-AMS; Aerodyne Research Inc.; abbreviated as AMS hereafter). Tracer fragments for each  $^{13}$ C-labeled dicarboxylic acid were thereby obtained (Table 1).

## 2.2. Gas-Phase Uptake.

A schematic diagram of experimental setup is shown in Figure 1. The setup consisted of four major components, including producing organic PM, generating gas-phase dicarboxylic acids, uptake of gas-phase molecules to the organic PM, and particle-phase measurements.

Organic PM was produced by the dark ozonolysis of α-pinene in the Harvard Environmental Chamber (HEC; 4.7 m³ in volume; 4.5 h residence time), which is a continuously mixed flow reactor (CMFR).³8,39 The HEC was operated at 22 °C and 40 % RH. Gaseous α-pinene was generated by evaporation of liquid α-pinene (99%, Sigma-Aldrich) delivered using a syringe pump (model Fusion-200, Chemyx Inc., Stafford, TX, USA) into a flow of zero air (1 L min<sup>-1</sup>). The α-pinene concentration was 22 ppb in the HEC before ozonolysis. Ozone was produced at 300 ppb in the HEC by passing a flow of zero air (1 L min<sup>-1</sup>) through an ultraviolet lamp (model

600, Jelight). Ozone was monitored using a photometric ozone analyzer (model 400E, Teledyne). The production of organic PM was initiated by turning on the ozone lamp. PM mass concentrations in the HEC reached a steady state prior to the uptake experiments.

The gas-phase probe molecules were produced using a nebulizer, in which the aqueous solution (0.1 g L<sup>-1</sup>) of each dicarboxylic acid was delivered using a syringe pump (model Fusion-200, Chemyx Inc., Stafford, TX, USA; liquid flow rate: 0.02 to 0.1 mL h<sup>-1</sup>) into a concentric quartz nebulizer (Meinhard A3, PerkinElmer Inc., Waltham, MA, USA) using a flow of zero air at 1 L min<sup>-1</sup>. The nebulized probe molecules were further diluted with a flow of zero air (0.1 L min<sup>-1</sup>). Unlike the experiments of identifying tracer fragments, the injected aqueous solution in the nebulizer and the dilution were such that full evaporation occurred into the gas-phase (i.e., below gas-phase saturation). As a secondary check, the flow further passed through a filter (Zeflour PTFE membrane, 47 mm diameter, 2 µm pore size, Pall Corp.) to remove any possible particles before entering into a second CMFR. Gas-phase concentrations of dicarboxylic acids prior to uptake were calculated based on mass balance of the nebulized aqueous solutions and the subsequent dilution flow.

For the uptake experiments, a portion (1.5 L min<sup>-1</sup>) of the organic PM outflow from the HEC was sampled. The flow was first passed through an ozone scrubber to prevent further oxidation reactions, and it was then directed to a humidity control system<sup>18</sup> with feedback regulation to adjust the RH. Further downstream, the uptake experiments took place. The flow was mixed with gas-phase isotopically labeled <sup>13</sup>C-dicarboxylic acid molecules in the second CMFR (a 7-L glass Erlenmeyer flask; residence time of 200 s) for exposure and uptake. The outflow from this CMFR was sampled by the AMS, a scanning mobility particle sizer (SMPS; TSI Inc.), and a condensation particle counter (CPC; model 3010, TSI Inc.). These instruments

together provided information on PM chemical composition and PM diameter-number distributions. Within a single experiment, the PM mass concentration was constant within  $\pm$  0.8  $\mu g$  m<sup>-3</sup>. Across the entire experimental set, the mass concentration of organic PM ranged from 8 to 12  $\mu g$  m<sup>-3</sup> in the outflow of the second CMFR. The diameter-number distribution of the particle population was lognormally distributed. The geometric mean diameters ranged from 201 to 295 nm. The particle number concentration and the surface area concentration ranged from 1603 to 1948 cm<sup>-3</sup> and 234 to 317  $\mu m^2$  cm<sup>-3</sup>, respectively.

AMS data were processed using the standard ToF-AMS data analysis toolkits (SQUIRREL v1.57I and PIKA v1.61I). A collection efficiency of unity was used in the data analysis. The  $^{13}$ C-labeled tracer fragments of the probe compounds were unconstrained from their isotopic abundance for fitting the high-resolution mass spectra in PIKA. The signal intensities of background fragments contributed by the isotope abundance of  $\alpha$ -pinene-derived organic PM were calculated manually based on the mass ratios compared to those of the primary fragments. The background signal intensities were then subtracted from the fitted absolute signal intensities of the  $^{13}$ C-labeled tracer fragments.

In individual experiments, the uptake of gas-phase probe molecules by α-pinene-derived organic PM was conducted for 6 h at different values of RH. The results presented here were obtained from the last 2 h of each experiment at steady state. A full list of the uptake experiments is summarized in Table 2. Uptake experiments of <sup>13</sup>C-labeled oxalic and malonic acids were conducted for variable gas-phase concentrations (Exp. 1 to 6 in Table 2). The gas-phase concentrations of the dicarboxylic acid molecules inside the second CMFR prior to uptake are listed in Table 2.

#### 3. RESULTS AND DISCUSSION

## 3.1. Uptake of Gas-Phase Probe Molecules by Organic PM.

The AMS-derived mass spectra of the four <sup>13</sup>C-labeled dicarboxylic acids in the particle phase are shown in Figure 2. For comparison, the mass spectra of the unlabeled compounds from the standard reference database of National Institute of Standards and Technology (NIST; https://webbook.nist.gov/chemistry/) are also plotted on the right. The mass spectra of <sup>13</sup>C-labeled oxalic, malonic, α-ketoglutaric, and adipic acids have prominent signal intensities of the <sup>13</sup>CO<sub>2</sub><sup>+</sup> fragment at *m/z* 45. This feature is similar to that of the unlabeled compounds but shifted by 1 Da for the <sup>13</sup>C-labeling. The mass spectral profiles are also consistent with those reported previously for the thermal decarboxylation of dicarboxylic acids, which produce high signal intensities at *m/z* 44 and arise mainly from the CO<sub>2</sub><sup>+</sup> fragment. <sup>40,41</sup> Another feature in Figure 2 is that more numerous fragments are produced for an increasing number of carbon atoms in the probe compounds, and correspondingly the average signal intensity decreases as the number of fragments increases. The primary tracer fragments for each of the dicarboxylic acid compounds are listed in Table 1. These tracer fragments are utilized in the analysis for characterizing the uptake of probe molecules to the organic PM.

Results for the uptake of gas-phase  $^{13}$ C-labeled dicarboxylic acids to  $\alpha$ -pinene-derived organic PM are shown in Figure 3. The mass fraction of the dicarboxylic acid tracer fragments in the total mass concentration of the organic PM is plotted for each probe molecule as a function of RH. The mass fractions increased monotonically with RH from 15% to 80% for oxalic, malonic, and  $\alpha$ -ketoglutaric acids (Figure 3a–c). The primary fragment  $^{13}$ CO<sub>2</sub><sup>+</sup> increased by a factor of 6.8, 9.5, and 25.1 for each of these acids, respectively, for the highest compared to the lowest RH.

In contrast to the other three acids, no systematic change was observed for the mass fraction of adipic acid tracer fragments with increasing RH (Figure 3d). This acid has the highest molar mass, lowest volatility, and expected lowest diffusivity among the studied probe molecules (Table 1), and each of these factors could contribute to the observations. The low volatility of adipic acid implies a low gas-phase concentration prior to uptake and thus low uptake. Furthermore, some  $^{12}$ C fragments of the  $\alpha$ -pinene-derived organic PM can contribute in small part to the signal intensity at the same m/z value, and in this case the signal intensities of the  $^{13}$ C tracer fragments could be too weak to distinguish. Another possibility is that surface adsorption at low RH already considerably depleted the gas-phase reservoir so that there was little further mass to undergo absorption at higher RH. Finally, another possibility is that this large molecule, which was the largest of the probe molecules, had sufficiently low diffusivity even at the highest studied RH that absorption did not occur to a significant extent during the time period of the experiments.

Oxalic and malonic acids were used to further test the relationship between the initial gasphase concentration of the probe molecules and the uptake amount to the particle phase (Figure 4). For oxalic acid at 80% RH, the mass fraction of the tracer fragment <sup>13</sup>CO<sub>2</sub><sup>+</sup> increased by a factor of 4 at the highest (66 ppb) compared to the lowest gas-phase concentrations (20 ppb), representing a factor of 3.3 increase in the gas-phase concentrations. By comparison, the factor was 2 at 10% RH. For malonic acid at 80% RH, the increase was 8.5 times at 19 ppb compared to 4 ppb, representing a factor of 4.8 increase in the gas-phase concentrations. At 10% RH, the increase in the fraction was < 10<sup>-4</sup>. Taken together, an absence of a plateau in the RH-dependent uptake curves in Figures 3 and 4 suggests that saturated uptake, representing the thermodynamic upper limit, was not reached even at 80% RH. Kinetic limitations from low diffusivity thus

continued to be important for the studied particle sizes (250 nm in geometric mean diameter) and observation times (200 s). Another possibility is that the equilibrium constant shifted with particle water content, but given the relatively small mass fraction of water, this explanation appears not plausible (see further analysis below related to Figure 5).

### 3.2. Influence of the Physical State of Organic PM.

230

231

232

233

234

235

236

237

238

239

240

241

242

243

244

245

246

247

248

249

250

251

252

The physical state of organic PM and its connections to molecular diffusivity are important governing factors in the uptake process, as explained below. The mass fractions of the main fragments C<sub>2</sub>H<sub>3</sub><sup>+</sup>, C<sub>2</sub>H<sub>3</sub>O<sup>+</sup>, and C<sub>4</sub>H<sub>7</sub><sup>+</sup> of α-pinene-derived organic PM were nearly constant or decreased slightly with increasing RH in all experiments (Figure S1 in Supporting Information). Increases in the mass fractions of <sup>13</sup>C tracer fragments with RH are therefore attributed to the enhanced uptake of the labeled dicarboxylic acids to the organic PM (Figure 3). Relative humidity is a dominant factor governing the physical state of organic PM because higher water chemical potentials in the gas phase drive water absorption by the condensed phase. Higher liquid water content logarithmically decreases the viscosity of the organic PM (right axis, Figure 7, section 3.3).<sup>7,12,42</sup> For α-pinene ozonolysis-derived organic PM, the transition from semisolid to liquid viscosity occurs at 70 to 85% RH based on particle rebound, although increased diffusivity and uptake can occur at lower RH. 12,18,43 After uptake, miscibility rather than phase separation was expected for the experimental conditions because the uptake was > 100 times less than the mass concentrations of the host PM matrix, and the carboxylic acid functionalities of the probe molecules are similar to functionalities already in the PM. This case differs from the conditions of some previous reports of phase separation, for which the two organic materials were in comparable amounts and these amounts were higher than the miscibility of one in the other.9,44

For the RH range of 15 to 80% of the current study, the viscosity of the α-pinene-derived PM decreases monotonically and logarithmically with increasing RH, thereby also changing condensed-phase diffusivity and increasing the rate of uptake when absorption was active (i.e., miscibility).<sup>7</sup> For a small molecule like NH<sub>3</sub>, a cross-over from kinetic limitations associated with low diffusivity to thermodynamic limitations on uptake occurs between 35 and 45% RH.<sup>18</sup> For a medium-sized molecule like levoglucosan, the cross-over also occurs in the same RH range, as explained by the logarithmic change in viscosity with RH.<sup>20</sup> The absence of saturation in the uptake in Figures 3a–3c, which differs from the results for NH<sub>3</sub> and levoglucosan, suggests that kinetic limitations tied to decreased diffusivity remain in place for the studied dicarboxylic acids, even up to 80% RH. The implication is that thermodynamic saturation was not reached during the exposure time (200 s) of these experiments.

An alternative explanation could be that the equilibrium constant for thermodynamic saturation shifts with greater water content, thus leading to greater uptake at higher RH. <sup>45,46</sup> This possible alternative explanation, however, can be ruled out because the estimated enhanced thermodynamic uptake associated solely with water appears too low to account for the observed results, as follows. The partitioning of a probe species between the gas and particle phases can be described by the equilibrium partitioning coefficient  $K_p$  (m³  $\mu$ g⁻¹): <sup>47,48</sup>

$$K_{\rm p} = \frac{C_{\rm p}}{M C_{\rm g}} \tag{1}$$

where  $C_p$  and  $C_g$  are the particle- and gas-phase concentrations of the probe species partitioned between the two phases ( $\mu g \text{ m}^{-3}$ ), and M is the total mass concentration of the absorbing phase ( $\mu g \text{ m}^{-3}$ ). For ideal thermodynamic behavior, the partitioning coefficient of a probe species is the inverse of its saturation concentration  $C^*$ , meaning  $K_p = 1 / C^*$ . For an assumption that liquid water is solely the absorbing matrix, the partitioned fraction of the probe species into the liquid

water can be represented as  $F_{\text{water}} = C_p / (C_p + C_g)$ , and the remaining fraction of the probe species in the gas phase can be represented as  $(1 - F_{\text{water}}) = C_g / (C_p + C_g)$ . Therefore, for partitioning of probe molecules associated solely with liquid water, the following functional form is obtained according to eq 1:

$$\frac{1}{C^*} = \frac{F_{\text{water}}}{M_{\text{water}} \left(1 - F_{\text{water}}\right)} \tag{2}$$

where  $M_{\text{water}}$  is the mass concentration of liquid water (µg m<sup>-3</sup>). The partitioned fraction of the probe species into liquid water can thus be calculated as follows:

$$F_{\text{water}} = \frac{M_{\text{water}}/C^*}{1 + M_{\text{water}}/C^*} \tag{3}$$

Quantity  $M_{\text{water}}$  can be estimated from the changes with RH in particle volume concentration based on the SMPS measurements. In this calculation, particles are taken as spherical, and the increased particle volume concentration is assumed to result solely from the absorbed liquid water content. By this method, the liquid water content accounted for up to 25–33% of the total particle mass at the highest RH (80%) in the studied conditions. This result is consistent with a growth factor of approximately 1.07 at 84% RH for particles of  $\alpha$ -pinene-ozonolysis-derived organic PM and diameters of 50 to 120 nm, as reported in ref 49. This growth factor corresponds to 15% by mass of liquid water for an organic PM density of 1.3 g cm<sup>-3</sup>.

Results of the calculations are shown in Figure 5. The mass fractions of the dicarboxylic acids are plotted for the partitioning associated with liquid water compared to that with organic PM (i.e.,  $F_{\text{water}}$  and  $F_{\text{organic}}$ , respectively) as well as their sum as the total partitioning  $F_{\text{total}}$  in the particle phase. The quantity  $F_{\text{total}}$  was obtained from the ratio of the total mass uptake in the particle phase compared to the mass concentration of probe molecules in both gas- and particle-phases. The total mass uptake in the particle phase was estimated based on the fractions of

primary tracer fragments in the mass spectra of pure <sup>13</sup>C-labeled dicarboxylic acids (Figure 2) multiplied by the total organic PM mass concentration measured by the AMS. The  $F_{\text{organic}}$  was then calculated from the difference between  $F_{\text{total}}$  and  $F_{\text{water}}$ . The partitioned fractions  $F_{\text{water}}$  of probe molecules into liquid water at the 80% RH are estimated as 0.3%, 3.5%, and 2.8% for oxalic, malonic, and  $\alpha$ -ketoglutaric acids, respectively, under the conditions of Figure 3. These values are much lower than  $F_{\text{total}}$  of 6.9%, 18.9%, and 24.1%, respectively. The partitioned fractions F<sub>water</sub> in a hypothetical case of solely liquid water are lower when accounting for a decrease in the activity coefficients of dicarboxylic acid molecules in the mixture matrix of organic PM and liquid water with increasing RH (Figure S2 in Supporting Information). The relevant inferences are that the association of dicarboxylic acids with liquid water in the particles did not contribute substantially to the uptake and hence the thermodynamic saturation point for the uptake did not shift appreciably with RH, implying that kinetic limitations to the uptake remained even to the highest studied RH. Therefore, the enhanced uptake of the probe molecules with increasing RH resulted primarily from the changes in the viscosity of the organic PM and the corresponding faster diffusivity of the probe molecules in the condensed phase.

## 3.3. Volatility and diffusivity of probe molecules.

298

299

300

301

302

303

304

305

306

307

308

309

310

311

312

313

314

315

316

317

318

319

320

The uptake of gas-phase molecules to PM takes place in several sequential steps, including gas-phase diffusion to the particle surface, thermal accommodation with the surface, possible reactions at the gas-particle interface, mass transfer across the liquid or semisolid surface, solvation, and diffusion and possible reaction with the particle.<sup>25,50</sup> The uptake process is affected both individually and collectively by the diffusing probe molecules and the host PM matrix. Nevertheless, given that conditions for producing organic PM remained the same across the series of experiments, the observed differences in the uptake of each probe species to the

organic PM can be connected to the differences among the probe molecules themselves. Furthermore, the possibility of chemical reactions between the probe molecules and the host PM matrix appears not to be a major factor because of the similar fractions of unlabeled primary fragments and thus the similar mass spectra of organic PM among the experiments (Figure S1). Species volatility can be one of the critical factors governing the uptake process.<sup>8,51</sup> According to the gas-particle partitioning described by Eq 1, the mass concentration of the probe molecules within the organic PM is the inverse of their volatility, as expressed by the vapor pressure. The uptake of dicarboxylic acids in the present study follows this trend in terms of the volatility dependence. Figures 6a and 6b present the total uptake of the labeled dicarboxylic acids as functions of relative humidity and vapor pressure, respectively. The gas-phase concentration prior to uptake was approximately the same among these experiments based on the mass balance of the nebulized aqueous solutions and the subsequent dilution flow, specifically 20, 19, and 14 ppb for oxalic, malonic, and  $\alpha$ -ketoglutaric acids, respectively (cf. Table 2). The uptake of these respective species increased stepwise with RH, reaching 5 to 15 times more at 80% RH compared to 15% RH (Figure 6a). The lowest uptake was for oxalic acid at each RH, and of the three probe molecules it had the highest volatility (Figure 6b). The uptake amounts of the other two probe molecules were similar to one another, and correspondingly their volatilities are similar (Figure 6b). Results from the uptake of levoglucosan<sup>20</sup> are also plotted in Figure 6 for comparison. The uptake (0.028 µg m<sup>-3</sup> at 80 % RH) was much less than that of dicarboxylic acids despite a vapor pressure  $(1.35 \times 10^{-4} \, \text{Pa})$  of 10 to 100 times lower than the probe molecules, but the gas-phase concentration of levoglucosan was 0.2 ppb in those experiments.<sup>20</sup> For an assumption of linear scaling with gas-phase concentration from 0.2 to 20 ppb for

321

322

323

324

325

326

327

328

329

330

331

332

333

334

335

336

337

338

339

340

341

342

343

comparison to the experiments of this study, the projected uptake is significantly more (2.8 µg

 $m^{-3}$ ), in line with the lower vapor pressure of this molecule. Levoglucosan also has lower solubility in the PM host matrix and thus achieves the limit of thermodynamic uptake at high RH during the exposure time (200 s).<sup>20</sup>

The uptake process can also be kinetically limited by a slow diffusion from the particle surface throughout the particle interior. Here we examine the possible effect of molecular size on the diffusivity of probe species. For medium-sized molecules diffusing within a matrix of organic PM that has similar molecular sizes and is not in a glassy state, the Stokes-Einstein relation is applicable for linking the diffusivity of probe molecules to the viscosity of organic PM matrix.  $^{18,19,52}$  In this case, the diffusion coefficient  $D_{\text{org}}$  of the probe molecules is represented as follows:  $^{53}$ 

$$D_{\text{org}} = \frac{kT}{6\pi r_{\text{m}}\eta} \tag{4}$$

where k is Boltzmann's constant, T is temperature,  $r_{\rm m}$  is the effective molecular radius, and  $\eta$  is the dynamic viscosity of the host matrix. The time for mixing throughout the particle interior was calculated as a function of particle diameter  $d_{\rm p}$  and diffusion coefficient  $D_{\rm org}$  by the following relation:<sup>54</sup>

$$\tau_{\text{mix}} = \frac{d_{\text{p}}^2}{4\pi^2 D_{\text{org}}} = \frac{3d_{\text{p}}^2 \eta r_{\text{m}}}{2\pi kT}$$
 (5)

The equation shows that the mixing time is proportional to the molecular radius  $r_{\rm m}$  of the probe species. The functional form of  $\tau_{\rm mix}$  in relation to  $r_{\rm m}$  and  $\eta$  is visualized in Figure 7. The molecular radii of oxalic, malonic, and  $\alpha$ -ketoglutaric acids were calculated as 0.25, 0.27, and 0.31 nm, respectively, from the van-der-Waals volume by addition of atomic increments and assuming a spherical molecule. The viscosity of  $\alpha$ -pinene-derived organic PM at variable RH was obtained from the literature. The viscosity of  $\alpha$ -pinene-derived organic PM at variable RH

For an increase in the molecular radius  $r_m$ , the diffusivity of the probe molecules decreases, and the mixing time within the organic PM is longer along isopleths of RH (dashed lines, Figure 7). A longer particle mixing time leads to less uptake when in a kinetically governed regime for all other factors held constant. Oxalic acid has the smallest molecular radius and thus the shortest mixing time among the studied probe molecules (Figure 7). Even so, it undergoes less uptake than malonic and  $\alpha$ -ketoglutaric acids (Figure 6). The explanation is that uptake is a combination of a sufficiently long exposure time relative to the mixing time and a sufficiently low vapor pressure to drive substantial uptake. In this case, Figure 7 suggests a shift in mixing times for oxalic acid to  $\alpha$ -ketoglutaric acid by a factor of 1.2 for an exposure time of 200 s, whereas Table 1 shows a shift in vapor pressure by a factor of 0.07. Thus, in this particular instance, the difference in vapor pressures proves more important than the difference in particle mixing times with regard to total uptake.

In summary, an isotopic labeling approach in this study distinguished the probe species in the particle phase from the host matrix of the organic PM. Particle physical state, reflected in a relative-humidity dependent viscosity, was the key governing factor in the uptake of dicarboxylic acid molecules to α-pinene ozonolysis-derived organic PM. Co-adsorbed water had a minor influence as an absorbing medium. Up to 80% RH, which was the highest RH of the study, thermodynamic saturation was not reached for the uptake of the semivolatile dicarboxylic acids for the studied conditions. The uptake of dicarboxylic acids differs from the results reported in the literature for ammonia and levoglucosan for a similar PM host matrix, as explained by their lower saturation concentrations in the PM matrix. <sup>18,20</sup> The monotonically increasing uptake of dicarboxylic acids reported herein is distinct from the behavior of probe species without diffusion limitation. <sup>9,34</sup> The differences among these studies might relate to the properties of the

semivolatile probe species, such as their molecular structures and functional groups, although the possible effect of different experimental conditions (e.g., the mass concentrations and mixing timescales) should also be considered. <sup>56</sup> α-Pinene ozonolysis-derived organic PM was used as the host matrix in the current study, and related interactions using organic PM produced from other gas-phase precursors and different reaction chemistry should be studied thoroughly to evaluate and extend the findings with regard to particle physical state and their significance in the atmosphere. Semivolatile probe organic species of various molecular structures and other functional groups also warrant further study for a comprehensive understanding of the relationships between the diffusivity and the physicochemical properties of the probe species. Additional quantitative characterization of the kinetic limitations associated with particle physical state can be obtained by carrying out experiments using size-selected organic PM for variable exposure times.

#### **ACKNOWLEDGMENTS**

This work was funded by the Office of Science of the U.S. Department of Energy (Grant DE-SC0012792) and the Division of Atmospheric and Geospace Sciences of the U.S. National Science Foundation (Grant 1640378).

### **SUPPORTING INFORMATION**

Figure S1 and Figure S2.

The Supporting Information is available free of charge on the ACS Publications website.

### REFERENCES

(1) Zhang, Q.; Jimenez, J. L.; Canagaratna, M. R.; Allan, J. D.; Coe, H.; Ulbrich, I.; Alfarra,

- M. R.; Takami, A.; Middlebrook, A. M.; Sun, Y. L.; Dzepina, K.; Dunlea, E.; Docherty,
- 413 K.; DeCarlo, P. F.; Salcedo, D.; Onasch, T.; Jayne, J. T.; Miyoshi, T.; Shimono, A.;
- Hatakeyama, S.; Takegawa, N.; Kondo, Y.; Schneider, J.; Drewnick, F.; Borrmann, S.;
- Weimer, S.; Demerjian, K.; Williams, P.; Bower, K.; Bahreini, R.; Cottrell, L.; Griffin, R.
- J.; Rautiainen, J.; Sun, J. Y.; Zhang, Y. M.; Worsnop, D. R. Ubiquity and Dominance of
- Oxygenated Species in Organic Aerosols in Anthropogenically-Influenced Northern
- Hemisphere Midlatitudes. *Geophys. Res. Lett.* **2007**, *34*, L13801.
- 419 (2) Hallquist, M.; Wenger, J. C.; Baltensperger, U.; Rudich, Y.; Simpson, D.; Claeys, M.;
- Dommen, J.; Donahue, N. M.; George, C.; Goldstein, A. H.; Hamilton, J. F.; Herrmann,
- 421 H.; Hoffmann, T.; Iinuma, Y.; Jang, M.; Jenkin, M. E.; Jimenez, J. L.; Kiendler-Scharr,
- 422 A.; Maenhaut, W.; McFiggans, G.; Mentel, T. F.; Monod, A.; Prévôt, A. S. H.; Seinfeld, J.
- 423 H.; Surratt, J. D.; Szmigielski, R.; Wildt, J. The Formation, Properties and Impact of
- Secondary Organic Aerosol: Current and Emerging Issues. *Atmos. Chem. Phys.* **2009**, 9,
- 425 5155–5236.
- 426 (3) Shrivastava, M.; Cappa, C. D.; Fan, J.; Goldstein, A. H.; Guenther, A. B.; Jimenez, J. L.;
- Kuang, C.; Laskin, A.; Martin, S. T.; Ng, N. L.; Petaja, T.; Pierce, J. R.; Rasch, P. J.;
- Roldin, P.; Seinfeld, J. H.; Shilling, J.; Smith, J. N.; Thornton, J. A.; Volkamer, R.; Wang,
- J.; Worsnop, D. R.; Zaveri, R. A.; Zelenyuk, A.; Zhang, Q. Recent Advances in
- 430 Understanding Secondary Organic Aerosol: Implications for Global Climate Forcing. *Rev.*
- 431 *Geophys.* **2017**, *55*, 509–559.
- 432 (4) Virtanen, A.; Joutsensaari, J.; Koop, T.; Kannosto, J.; Yli-Pirilä, P.; Leskinen, J.; Mäkelä,
- J. M.; Holopainen, J. K.; Pöschl, U.; Kulmala, M.; Worsnop, D. R.; Laaksonen, A. An
- 434 Amorphous Solid State of Biogenic Secondary Organic Aerosol Particles. *Nature* **2010**,

- 435 467, 824–827.
- 436 (5) Bateman, A. P.; Gong, Z.; Liu, P.; Sato, B.; Cirino, G.; Zhang, Y.; Artaxo, P.; Bertram, A.
- 437 K.; Manzi, A. O.; Rizzo, L. V.; Souza, R. A. F.; Zaveri, R. A.; Martin, S. T. Sub-
- 438 Micrometre Particulate Matter Is Primarily in Liquid Form over Amazon Rainforest. *Nat.*
- 439 *Geosci.* **2016**, *9*, 34–37.
- 440 (6) Kuwata, M.; Martin, S. T. Phase of Atmospheric Secondary Organic Material Affects Its
- 441 Reactivity. *Proc. Natl. Acad. Sci.* **2012**, *109*, 17354–17359.
- 442 (7) Renbaum-Wolff, L.; Grayson, J. W.; Bateman, A. P.; Kuwata, M.; Sellier, M.; Murray, B.
- J.; Shilling, J. E.; Martin, S. T.; Bertram, A. K. Viscosity of α-Pinene Secondary Organic
- Material and Implications for Particle Growth and Reactivity. *Proc. Natl. Acad. Sci. U. S.*
- *A.* **2013**, *110*, 8014–8019.
- 446 (8) Liu, P.; Li, Y. J.; Wang, Y.; Gilles, M. K.; Zaveri, R. A.; Bertram, A. K.; Martin, S. T.
- Lability of Secondary Organic Particulate Matter. *Proc. Natl. Acad. Sci. U. S. A.* **2016**,
- 448 *113*, 12643–12648.
- 449 (9) Ye, Q.; Robinson, E. S.; Ding, X.; Ye, P.; Sullivan, R. C.; Donahue, N. M. Mixing of
- 450 Secondary Organic Aerosols versus Relative Humidity. *Proc. Natl. Acad. Sci.* **2016**, *113*,
- 451 12649–12654.
- 452 (10) Reid, J. P.; Bertram, A. K.; Topping, D. O.; Laskin, A.; Martin, S. T.; Petters, M. D.;
- 453 Pope, F. D.; Rovelli, G. The Viscosity of Atmospherically Relevant Organic Particles.
- *Nat. Commun.* **2018**, *9*, 1–14.
- 455 (11) Slade, J. H.; Knopf, D. A. Multiphase OH Oxidation Kinetics of Organic Aerosol: The
- Role of Particle Phase State and Relative Humidity. *Geophys. Res. Lett.* **2014**, *41*, 5297–
- 457 5306.

- 458 (12) Bateman, A. P.; Bertram, A. K.; Martin, S. T. Hygroscopic Influence on the Semisolid-to-
- Liquid Transition of Secondary Organic Materials. J. Phys. Chem. A 2015, 119, 4386—
- 460 4395.
- 461 (13) O'Brien, R. E.; Neu, A.; Epstein, S. A.; MacMillan, A. C.; Wang, B.; Kelly, S. T.;
- Nizkorodov, S. A.; Laskin, A.; Moffet, R. C.; Gilles, M. K. Physical Properties of
- Ambient and Laboratorygenerated Secondary Organic Aerosol. *Geophys. Res. Lett.* **2014**,
- 464 41, 4347–4353.
- 465 (14) Pajunoja, A.; Malila, J.; Hao, L.; Joutsensaari, J.; Lehtinen, K. E. J.; Virtanen, A.
- Estimating the Viscosity Range of SOA Particles Based on Their Coalescence Time.
- 467 Aerosol Sci. Technol. **2014**, 48, i–iv.
- 468 (15) Zhang, Y.; Sanchez, M. S.; Douet, C.; Wang, Y.; Bateman, A. P.; Gong, Z.; Kuwata, M.;
- Renbaum-Wolff, L.; Sato, B. B.; Liu, P. F.; Bertram, A. K.; Geiger, F. M.; Martin, S. T.
- 470 Changing Shapes and Implied Viscosities of Suspended Submicron Particles. *Atmos*.
- 471 *Chem. Phys.* **2015**, *15*, 7819–7829.
- 472 (16) Perraud, V.; Bruns, E. A.; Ezell, M. J.; Johnson, S. N.; Yu, Y.; Alexander, M. L.;
- Zelenyuk, A.; Imre, D.; Chang, W. L.; Dabdub, D.; Pankow, J. F.; Finlayson-Pitts, B. J.
- Nonequilibrium Atmospheric Secondary Organic Aerosol Formation and Growth. *Proc.*
- 475 Natl. Acad. Sci. **2012**, 109, 2836–2841.
- 476 (17) Zelenyuk, A.; Imre, D.; Beránek, J.; Abramson, E.; Wilson, J.; Shrivastava, M. Synergy
- between Secondary Organic Aerosols and Long-Range Transport of Polycyclic Aromatic
- 478 Hydrocarbons. *Environ. Sci. Technol.* **2012**, *46*, 12459–12466.
- 479 (18) Li, Y. J.; Liu, P.; Gong, Z.; Wang, Y.; Bateman, A. P.; Bergoend, C.; Bertram, A. K.;
- 480 Martin, S. T. Chemical Reactivity and Liquid/Nonliquid States of Secondary Organic

- 481 Material. *Environ. Sci. Technol.* **2015**, *49*, 13264–13274.
- 482 (19) Liu, P.; Li, Y. J.; Wang, Y.; Bateman, A. P.; Zhang, Y.; Gong, Z.; Bertram, A. K.; Martin,
- 483 S. T. Highly Viscous States Affect the Browning of Atmospheric Organic Particulate
- 484 Matter. ACS Cent. Sci. 2018, 4, 207–215.
- 485 (20) Gong, Z.; Han, Y.; Liu, P.; Ye, J.; Keutsch, F. N.; McKinney, K.; Martin, S. T. Influence
- of Particle Physical State on the Uptake of Medium-Sized Organic Molecules. *Environ*.
- 487 *Sci. Technol.* **2018**, *52*, 8381–8389.
- 488 (21) Donahue, N. M.; Robinson, A. L.; Pandis, S. N. Atmospheric Organic Particulate Matter:
- From Smoke to Secondary Organic Aerosol. *Atmos. Environ.* **2009**, *43*, 94–106.
- 490 (22) Pankow, J. F. An Absorption-Model of the Gas Aerosol Partitioning Involved in the
- 491 Formation of Secondary Organic Aerosol. *Atmos. Environ.* **1994**, *28*, 189–193.
- 492 (23) Donahue, N. M.; Robinson, a. L.; Stanier, C. O.; Pandis, S. N. Coupled Partitioning,
- Dilution, and Chemical Aging of Semivolatile Organics. Environ. Sci. Technol. 2006, 40,
- 494 2635–2643.
- 495 (24) Abramson, E.; Imre, D.; Beránek, J.; Wilson, J.; Zelenyuk, A. Experimental
- Determination of Chemical Diffusion within Secondary Organic Aerosol Particles. *Phys.*
- 497 Chem. Chem. Phys. **2013**, 15, 2983–2991.
- 498 (25) Kolb, C. E.; Cox, R. A.; Abbatt, J. P. D.; Ammann, M.; Davis, E. J.; Donaldson, D. J.;
- Garrett, B. C.; George, C.; Griffiths, P. T.; Hanson, D. R.; Kulmala, M.; McFiggans, G.;
- Pöschl, U.; Riipinen, I.; Rossi, M. J.; Rudich, Y.; Wagner, P. E.; Winkler, P. M.;
- Worsnop, D. R.; O'Dowd, C. D. An Overview of Current Issues in the Uptake of
- Atmospheric Trace Gases by Aerosols and Clouds. *Atmos. Chem. Phys.* **2010**, *10*, 10561–
- 503 10605.

- 504 (26) Liggio, J.; Li, S. M. Reactive Uptake of Pinonaldehyde on Acidic Aerosols. J. Geophys.
- 505 Res. Atmos. **2006**, 111, 1–12.
- 506 (27) Fu, T. M.; Jacob, D. J.; Heald, C. L. Aqueous-Phase Reactive Uptake of Dicarbonyls as a
- Source of Organic Aerosol over Eastern North America. Atmos. Environ. 2009, 43, 1814—
- 508 1822.
- 509 (28) Galloway, M. M.; Chhabra, P. S.; Chan, A. W. H.; Surratt, J. D.; Flagan, R. C.; Seinfeld,
- J. H.; Keutsch, F. N. Glyoxal Uptake on Ammonium Sulphate Seed Aerosol: Reaction
- Products and Reversibility of Uptake under Dark and Irradiated Conditions. *Atmos. Chem.*
- 512 *Phys.* **2009**, *9*, 3331–3345.
- 513 (29) Kuwata, M.; Liu, Y.; McKinney, K.; Martin, S. T. Physical State and Acidity of Inorganic
- Sulfate Can Regulate the Production of Secondary Organic Material from Isoprene
- Photooxidation Products. Phys. Chem. Chem. Phys. 2015, 17, 5670–5678.
- 516 (30) Liu, Y. J.; Kuwata, M.; McKinney, K. A.; Martin, S. T. Uptake and Release of Gaseous
- Species Accompanying the Reactions of Isoprene Photo-Oxidation Products with Sulfate
- Particles. Phys. Chem. Chem. Phys. **2016**, 18, 1595–1600.
- 519 (31) Dommen, J.; Hellen, H.; Saurer, M.; Jaeggi, M.; Siegwolf, R.; Metzger, A.; Duplissy, J.;
- Fierz, M.; Baltensperger, U. Determination of the Aerosol Yield of Isoprene in the
- Presence of an Organic Seed with Carbon Isotope Analysis. *Environ. Sci. Technol.* **2009**,
- *43*, 6697–6702.
- 523 (32) Hildebrandt, L.; Henry, K. M.; Kroll, J. H.; Worsnop, D. R.; Pandis, S. N.; Donahue, N.
- M. Evaluating the Mixing of Organic Aerosol Components Using High-Resolution
- 525 Aerosol Mass Spectrometry. *Environ. Sci. Technol.* **2011**, *45*, 6329–6335.
- 526 (33) Hicks, R. K.; Day, D. A.; Jimenez, J. L.; Tolbert, M. A. Elemental Analysis of Complex

- Organic Aerosol Using Isotopic Labeling and Unit-Resolution Mass Spectrometry. *Anal.*
- 528 *Chem.* **2015**, *87*, 2741–2747.
- 529 (34) Ye, Q.; Upshur, M. A.; Robinson, E. S.; Geiger, F. M.; Sullivan, R. C.; Thomson, R. J.;
- Donahue, N. M. Following Particle-Particle Mixing in Atmospheric Secondary Organic
- Aerosols by Using Isotopically Labeled Terpenes. *Chem* **2018**, *4*, 318–333.
- 532 (35) Kawamura, K.; Bikkina, S. A Review of Dicarboxylic Acids and Related Compounds in
- 533 Atmospheric Aerosols: Molecular Distributions, Sources and Transformation. *Atmos. Res.*
- **2016**, *170*, 140–160.
- 535 (36) Booth, A. M.; Barley, M. H.; Topping, D. O.; McFiggans, G.; Garforth, A.; Percival, C. J.
- Solid State and Sub-Cooled Liquid Vapour Pressures of Substituted Dicarboxylic Acids
- Using Knudsen Effusion Mass Spectrometry (KEMS) and Differential Scanning
- 538 Calorimetry. *Atmos. Chem. Phys.* **2010**, *10*, 4879–4892.
- 539 (37) Robinson, A. L.; Donahue, N. M.; Shrivastava, M. K.; Weitkamp, E. a; Sage, A. M.;
- Grieshop, A. P.; Lane, T. E.; Pierce, J. R.; Pandis, S. N. Rethinking Organic Aerosols:
- Semivolatile Emissions and Photochemical Aging. *Science* **2007**, *315*, 1259–1262.
- 542 (38) Shilling, J. E.; Chen, Q.; King, S. M.; Rosenoern, T.; Kroll, J. H.; Worsnop, D. R.;
- McKinney, K. A.; Martin, S. T. Particle Mass Yield in Secondary Organic Aerosol
- Formed by the Dark Ozonolysis of α-Pinene. *Atmos. Chem. Phys.* **2008**, 8, 2073–2088.
- 545 (39) Han, Y.; Gong, Z.; Liu, P.; De Sá, S. S.; McKinney, K. A.; Martin, S. T. Influence of
- Particle Surface Area Concentration on the Production of Organic Particulate Matter in a
- 547 Continuously Mixed Flow Reactor. *Environ. Sci. Technol.* **2019**, *53*, 4968–4976.
- 548 (40) Aiken, A. C.; Decarlo, P. F.; Jimenez, J. L. Elemental Analysis of Organic Species with
- Electron Ionization High-Resolution Mass Spectrometry. **2007**, *79*, 8350–8358.

- 550 (41) Takegawa, N.; Miyakawa, T.; Kawamura, K.; Kondo, Y. Contribution of Selected
- Dicarboxylic and ω-Oxocarboxylic Acids in Ambient Aerosol to the m/z 44 Signal of an
- Aerodyne Aerosol Mass Spectrometer. *Aerosol Sci. Technol.* **2007**, *41*, 418–437.
- 553 (42) Hinks, M. L.; Brady, M. V.; Lignell, H.; Song, M.; Grayson, J. W.; Bertram, A. K.; Lin,
- P.; Laskin, A.; Laskin, J.; Nizkorodov, S. A. Effect of Viscosity on Photodegradation
- Rates in Complex Secondary Organic Aerosol Materials. *Phys. Chem. Chem. Phys.* **2016**,
- *18*, 8785–8793.
- 557 (43) Kidd, C.; Perraud, V.; Finlayson-Pitts, B. J. New Insights into Secondary Organic Aerosol
- from the Ozonolysis of α-Pinene from Combined Infrared Spectroscopy and Mass
- 559 Spectrometry Measurements. *Phys. Chem. Chem. Phys.* **2014**, *16*, 22706–22716.
- 560 (44) Gorkowski, K.; Donahue, N. M.; Sullivan, R. C. Emulsified and Liquid-Liquid Phase-
- Separated States of α-Pinene Secondary Organic Aerosol Determined Using Aerosol
- 562 Optical Tweezers. *Environ. Sci. Technol.* **2017**, *51*, 12154–12163.
- 563 (45) Ervens, B.; Kreidenweis, S. M. SOA Formation by Biogenic and Carbonyl Compounds:
- Data Evaluation and Application. *Environ. Sci. Technol.* **2007**, *41*, 3904–3910.
- 565 (46) Ervens, B.; Turpin, B. J.; Weber, R. J. Secondary Organic Aerosol Formation in Cloud
- Droplets and Aqueous Particles (AqSOA): A Review of Laboratory, Field and Model
- 567 Studies. Atmos. Chem. Phys. **2011**, 11, 11069–11102.
- 568 (47) Pankow, J. F. Review and Comparative Analysis of the Theories on Partitioning between
- the Gas and Aerosol Particulate Phases in the Atmosphere. Atmos. Environ. 1987, 21,
- 570 2275–2283.
- 571 (48) Seinfeld, J. H.; Pankow, J. F. Organic Atmospheric Particulate Material. *Annu. Rev. Phys.*
- 572 *Chem.* **2003**, *54*, 121–140.

- 573 (49) Virkkula, A.; Van Dingenen, R.; Raes, F.; Hjorth, J. Hygroscopic Properties of Aerosol
- Formed by Oxidation of Limonene, α-Pinene, and β-Pinene. J. Geophys. Res. Atmos.
- **1999**, *104*, 3569–3579.
- 576 (50) Berkemeier, T.; Huisman, A. J.; Ammann, M.; Shiraiwa, M.; Koop, T.; Pöschl, U. Kinetic
- Regimes and Limiting Cases of Gas Uptake and Heterogeneous Reactions in Atmospheric
- Aerosols and Clouds: A General Classification Scheme. Atmos. Chem. Phys. 2013, 13,
- 579 6663–6686.
- 580 (51) Shiraiwa, M.; Seinfeld, J. H. Equilibration Timescale of Atmospheric Secondary Organic
- Aerosol Partitioning. *Geophys. Res. Lett.* **2012**, *39*, 1–6.
- 582 (52) Shiraiwa, M.; Ammann, M.; Koop, T.; Pöschl, U. Gas Uptake and Chemical Aging of
- Semisolid Organic Aerosol Particles. *Proc. Natl. Acad. Sci. U. S. A.* **2011**, *108*, 11003–
- 584 11008.
- 585 (53) Edward, J. T. Molecular Volumes and the Stokes-Einstein Equation. J. Chem. Educ. 1970,
- 586 47, 261–270.
- 587 (54) Seinfeld, J. H.; Pandis, S. N. Atmospheric Chemistry and Physics: From Air Pollution to
- Climate Change (2nd Ed.). John Wiley Sons, Inc., Hoboken, New Jersey 2006.
- 589 (55) Bondi, A. Van Der Waals Volumes and Radii. J. Phys. Chem. **1964**, 68, 441–451.
- 590 (56) Grayson, J. W.; Zhang, Y.; Mutzel, A.; Renbaum-Wolff, L.; Böge, O.; Kamal, S.;
- Herrmann, H.; Martin, S. T.; Bertram, A. K. Effect of Varying Experimental Conditions
- on the Viscosity of α-Pinene Derived Secondary Organic Material. *Atmos. Chem. Phys.*
- **2016**, *16*, 6027–6040.

## **List of Tables**

Table 1. Physical and chemical properties of the probe <sup>13</sup>C-labeled dicarboxylic acids. The asterisks in the molecular structures represent <sup>13</sup>C labeling on all carbon atoms (i.e., full labeling). <sup>a</sup>Saturation concentrations were calculated from the vapor pressure at atmospheric conditions of 298 K and 101.325 kPa. The vapor pressures and saturation concentrations listed herein represent those of unlabeled regular compounds, and no significant differences are expected for the labeled ones. <sup>b</sup>The primary tracer fragments were derived from the mass spectra of pure probe compounds measured by the AMS.

	<sup>13</sup> C-isotopically labeled probe compounds			
compound	oxalic acid	malonic acid	α-ketoglutaric acid	adipic acid
molecular structure	HO * OH	но он	но	HO*****OH
chemical formula	$^{13}C_{2}H_{2}O_{4}$	$^{13}\text{C}_{3}\text{H}_{4}\text{O}_{4}$	$^{13}\text{C}_5\text{H}_6\text{O}_5$	$^{13}C_6H_{10}O_4$
molar mass (g mol <sup>-1</sup> )	92.02	107.04	151.06	152.10
chemical purity	≥ 98%	≥ 98%	≥ 90%	≥ 98%
vapor pressure (Pa) <sup>36</sup>	$2.74 \times 10^{-2}$	$3.19 \times 10^{-3}$	$2.02 \times 10^{-3}$	$2.14 \times 10^{-4}$
saturation concentration <sup>a</sup> (ppb, μg m <sup>-3</sup> )	270, 1018	31, 138	20, 123	2, 13
primary tracer fragments <sup>b</sup>	<sup>13</sup> C <sup>+</sup> , <sup>13</sup> CO <sub>2</sub> <sup>+</sup> , <sup>13</sup> CHO <sub>2</sub> <sup>+</sup>	<sup>13</sup> CO <sub>2</sub> <sup>+</sup> , <sup>13</sup> CHO <sub>2</sub> <sup>+</sup> , <sup>13</sup> C <sub>2</sub> H <sub>4</sub> O <sub>2</sub> <sup>+</sup>	<sup>13</sup> CO <sub>2</sub> <sup>+</sup> , <sup>13</sup> CHO <sub>2</sub> <sup>+</sup> , <sup>13</sup> C <sub>3</sub> H <sub>4</sub> O <sup>+</sup>	<sup>13</sup> CO <sub>2</sub> <sup>+</sup> , <sup>13</sup> CHO <sub>2</sub> <sup>+</sup> , <sup>13</sup> C <sub>4</sub> H <sub>7</sub> <sup>+</sup>

**Table 2.** List of conducted experiments for the uptake of gas-phase  $^{13}$ C-labeled dicarboxylic acids by organic PM produced from the dark ozonolysis of  $\alpha$ -pinene. Relative humidity in each experiment was increased stepwise from approximately 10% to 85%.

exp.	probe molecules	gas-phase concentration (ppb)
1	<sup>13</sup> C-oxalic acid	66
2	<sup>13</sup> C-oxalic acid	39
3	<sup>13</sup> C-oxalic acid	20
4	<sup>13</sup> C-malonic acid	19
5	<sup>13</sup> C-malonic acid	11
6	<sup>13</sup> C-malonic acid	4
7	<sup>13</sup> C-α-ketoglutaric acid	14
8	<sup>13</sup> C-adipic acid	< 2
9	None	n/a

## Figure captions

610

631

611 **Figure 1.** A schematic diagram of the experimental setup for the study of the uptake of <sup>13</sup>C-612 isotopically labeled dicarboxylic acid molecules to organic particulate matter produced 613 by the dark ozonolysis of α-pinene. The green circles in reactor 1 represent the organic 614 PM formed by  $\alpha$ -pinene ozonolysis. The blue circles and the green circles in reactor 2 615 represent the gas-phase dicarboxylic acid molecules and their uptake to organic PM, 616 respectively. Abbreviations: PM, particulate matter; HR-ToF-AMS, high-resolution 617 time-of-flight aerosol mass spectrometer; SMPS, scanning mobility particle sizer; and 618 CPC, condensation particle counter. 619 Figure 2. (a–d) High-resolution mass spectra obtained in this study by aerosolizing reference 620 solutions of <sup>13</sup>C-labeled oxalic, malonic, α-ketoglutaric, and adipic acids and 621 conducting measurements using the AMS. (e-h) Mass spectra of the corresponding 622 unlabeled compounds from the NIST standard reference database 623 (https://webbook.nist.gov/chemistry/). 624 Figure 3. Ratios of the mass concentrations of the primary tracer fragments of probe species in 625 the particle phase to the mass concentrations of total organic particulate matter as a function of relative humidity for <sup>13</sup>C-labeled (a) oxalic acid (OXA, 66 ppb), (b) 626 627 malonic acid (MA, 19 ppb), (c) α-ketoglutaric acid (KGA, 14 ppb), and (d) adipic acid (ADA, < 2 ppb). The results are corrected for AMS background. 628 Figure 4. Ratios of the mass concentrations of the tracer fragment <sup>13</sup>CO<sub>2</sub><sup>+</sup> in the particle phase to 629 630 the mass concentrations of total organic PM as a function of relative humidity for (a)

<sup>13</sup>C-labeled oxalic acid and (b) <sup>13</sup>C-labeled malonic acid at variable gas-phase

632 concentrations (for the experiments of 1 to 3 and 4 to 6 in Table 2, respectively). Other 633 tracer fragments of probe molecules exhibited similar trends (not shown). Figure 5. Fraction of <sup>13</sup>C-labeled dicarboxylic acid molecules partitioned to the particle phase 634 635 (i.e.,  $F_{\text{total}}$ ) relative to the total concentration in gas- and particle-phases for <sup>13</sup>C-labeled 636 (a) oxalic, (b) malonic, and (c) α-ketoglutaric acids (for the experiments of 3, 4, and 7 637 in Table 2, respectively). Also shown is the partitioning of  $F_{\text{total}}$  as separately 638 attributable to association with organic PM as  $F_{\text{organic}}$  and liquid water as  $F_{\text{water}}$  when 639 approximated by a linear mixing model (see main text). **Figure 6.** Mass concentrations of  $^{13}$ C-labeled oxalic, malonic, and  $\alpha$ -ketoglutaric acids 640 641 partitioned to the particle phase as a function of (a) relative humidity and (b) their 642 vapor pressures (for the experiments of 3, 4, and 7 in Table 2). The mass concentrations were estimated from the fractions of primary tracer fragments <sup>13</sup>CO<sub>2</sub><sup>+</sup> 643 and <sup>13</sup>CHO<sub>2</sub><sup>+</sup> in the total organic PM mass concentration and in pure compounds. For 644 comparison, results from Gong et al.<sup>20</sup> for the uptake of levoglucosan at a gas-phase 645 646 concentration of 0.2 ppb to  $\alpha$ -pinene-derived organic PM are also plotted. 647 Figure 7. Expected mixing time of probe molecules within a 250-nm particle as a function of the 648 molecular radius of the probe species based on the Stokes-Einstein relation. The 649 righthand ordinate shows the RH-dependent viscosity of α-pinene ozonolysis-derived organic PM reported at RH of 10–60%<sup>15</sup> and 70–90%<sup>7</sup> based on different approaches 650 651 in the literature.

# **List of Figures**

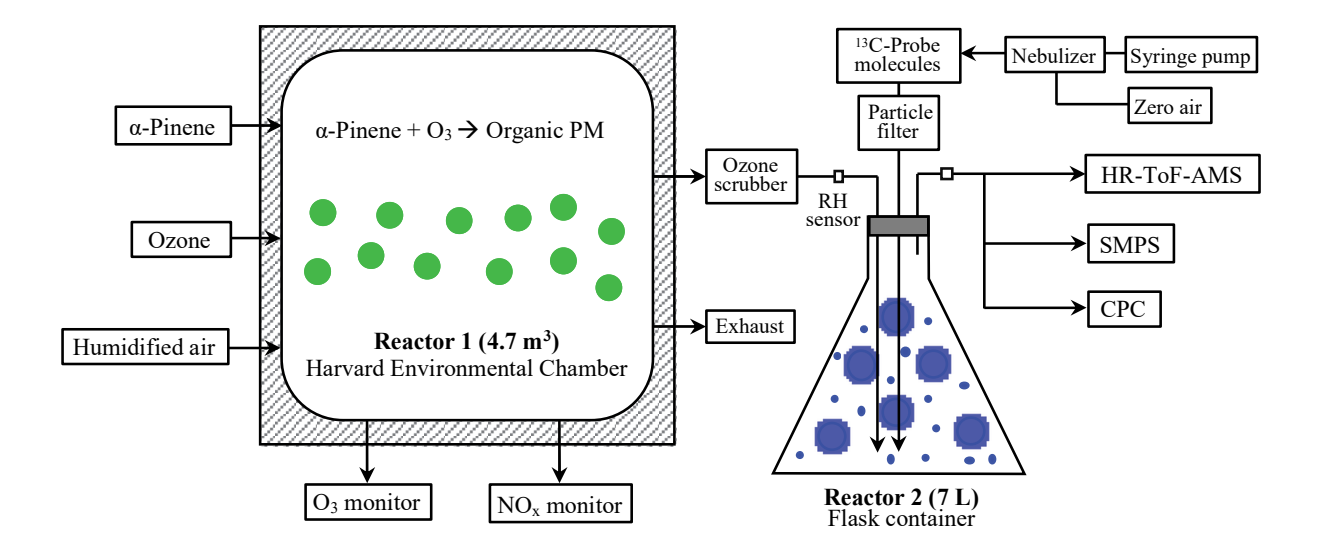
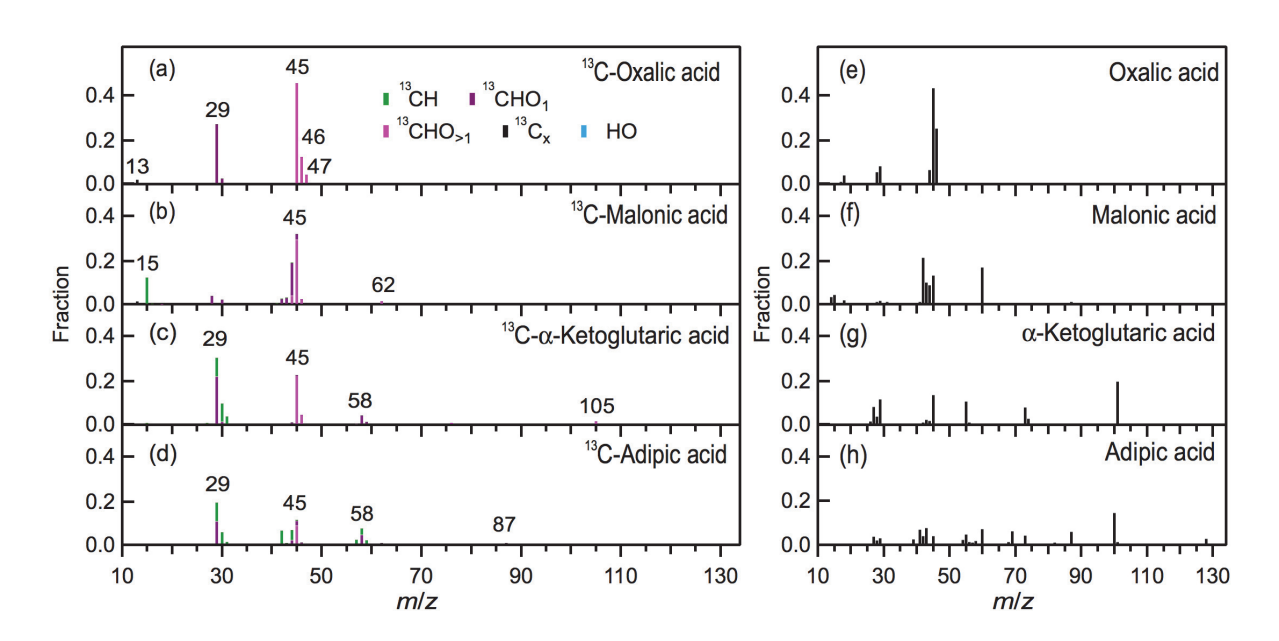
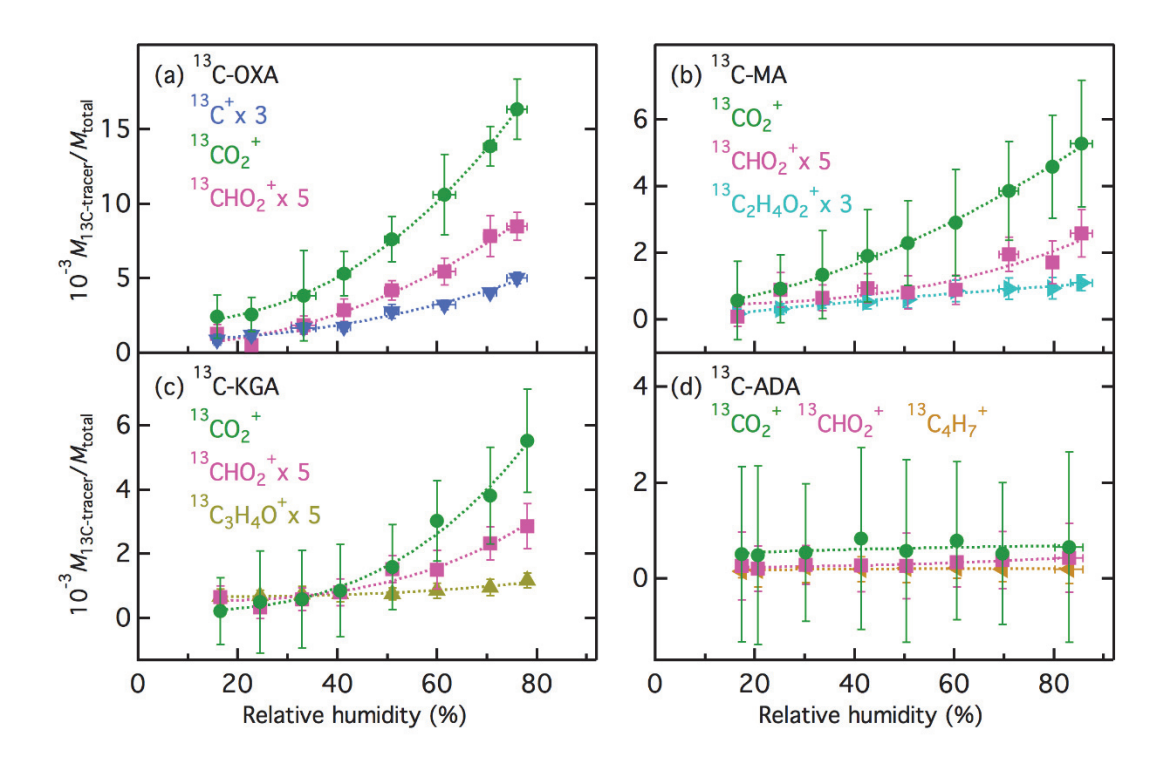


Figure 1.



659 Figure 2.



662 Figure 3.

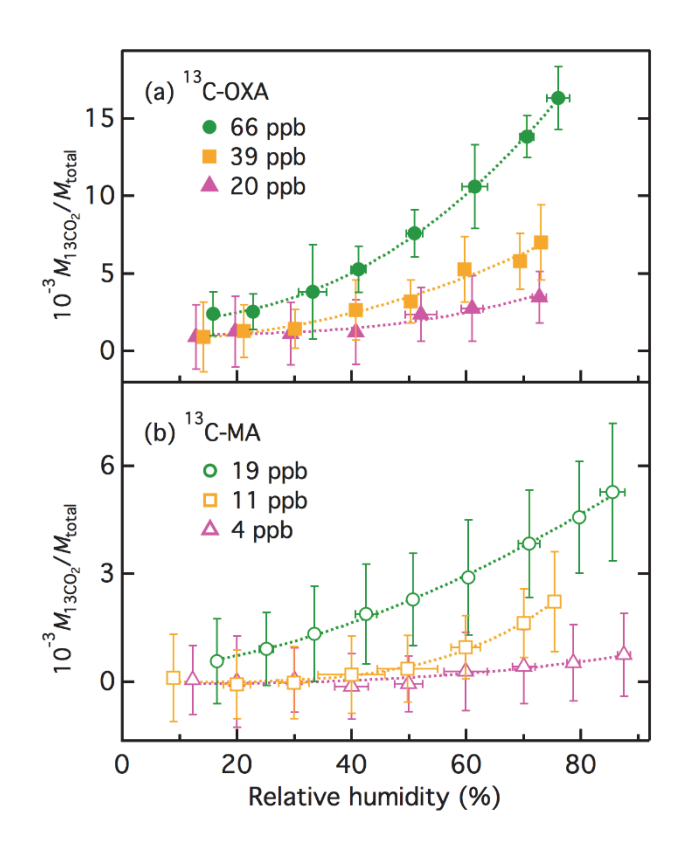


Figure 4.

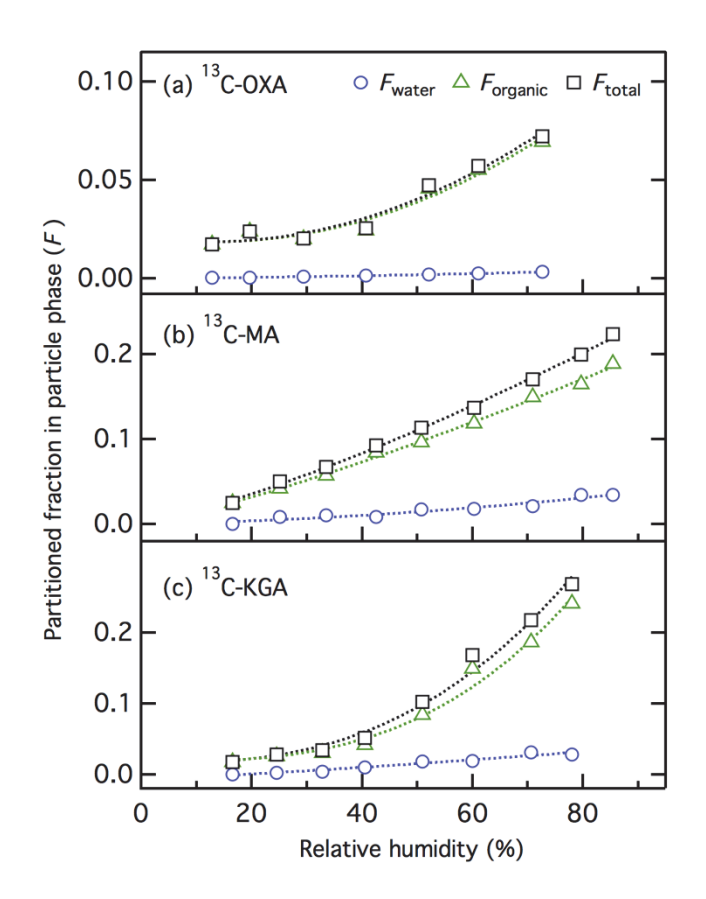
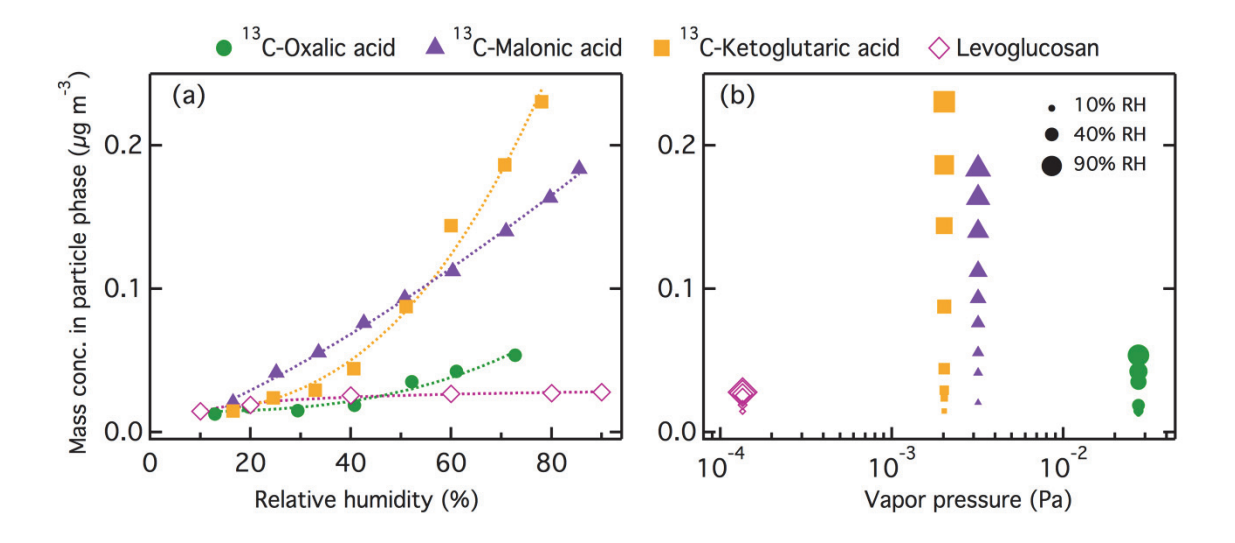


Figure 5.



**Figure 6.** 

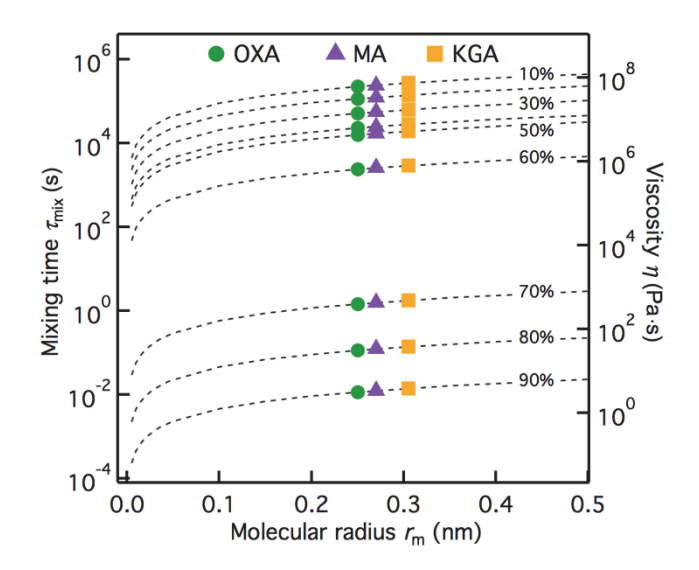


Figure 7.